Full Length Articles

Significant feed-forward connectivity revealed by high frequency components of BOLD fMRI signals

Fa-Hsuan Lin [a,b,1], Ying-Hua Chu [a,1], Yi-Cheng Hsu [a], Jo-Fu Lotus Lin [a], Kevin W.-K. Tsai [b], Shang-Yueh Tsai [c,d], Wen-Jui Kuo [e,*]

[a] Institute of Biomedical Engineering, National Taiwan University, Taipei, Taiwan
[b] Department of Neuroscience and Biomedical Engineering, Aalto University, Espoo, Finland
[c] Institute of Applied Physics, National Chengchi University, Taipei, Taiwan
[d] Research Center for Mind Brain and Learning, National Chengchi University, Taipei, Taiwan
[e] Institute of Neuroscience, National Yang-Ming University, Taipei, Taiwan

ARTICLE INFO

ABSTRACT

Granger causality analysis has been suggested as a method of estimating causal modulation without specifying the direction of information flow a priori. Using BOLD-contrast functional MRI (fMRI) data, such analysis has been typically implemented in the time domain. In this study, we used magnetic resonance inverse imaging, a method of fast fMRI enabled by massively parallel detection allowing up to 10 Hz sampling rate, to investigate the causal modulation at different frequencies up to 5 Hz. Using a visuomotor two-choice reaction-time task, both the spectral decomposition of Granger causality and isolated effective coherence revealed that the BOLD signal at frequency up to 3 Hz can still be used to estimate significant dominant directions of information flow consistent with results from the time-domain Granger causality analysis. We showed the specificity of estimated dominant directions of information flow at high frequencies by contrasting causality estimates using data collected during the visuomotor task and resting state. Our data suggest that hemodynamic responses carry physiological information related to inter-regional modulation at frequency higher than what has been commonly considered.

© 2015 Elsevier Inc. All rights reserved.

Introduction

Functional magnetic resonance imaging (fMRI) (Belliveau et al., 1991) using BOLD contrast (Kwong et al., 1992; Ogawa et al., 1992) has become an indispensable tool in non-invasive elucidation of brain areas subserving cognitive processes and behaviors. In addition to localizing individual functional areas, fMRI can also be used to reveal spatially distributed neuronal networks by studying either the temporal correlation (i.e., functional connectivity) or the causal modulation between brain areas (i.e., effective connectivity) activated by specific stimuli and tasks (for review, see (Friston, 2011b)).

The effective connectivity analysis of fMRI data has various implementations, including Structural Equation Modeling (SEM) (McArdle and McDonald, 1984), dynamic causal modeling (DCM) (Friston, 2011a; Friston et al., 2003; Penny et al., 2004), and Granger causality analysis (Granger, 1969). Different from SEM and DCM, where models of explicit directional influences among functional

areas must be specified a priori, Granger causality analysis uses fMRI data to estimate the direction of information flow directly. The inference about the direction of information flow in Granger causality analysis is based on the effectiveness of the 'prediction' (Granger, 1969). Specifically, if one region is considered as the 'source', the prediction of the behavior at the 'target' region should be significantly improved when information about the 'source' is provided. In practice, most Granger causality analyses use fMRI time series and time-domain models in these prediction calculations. While the validity of Granger causality estimates using fMRI has been either supported (Abler et al., 2006; Deshpande et al., 2009; Eichler, 2005; Goebel et al., 2003; Kayser et al., 2009; Londei et al., 2006; Roebroeck et al., 2005; Sato et al., 2006) or questioned (David et al., 2008; Smith et al., 2012) because of regional difference in vasculature reactivity (Lee et al., 1995; Miezin et al., 2000), Granger causality analysis has been applied to many fMRI studies (for review, see (Stephan and Roebroeck, 2012)).

Note that Granger causality can be also formulated in the frequency domain (Brovelli et al., 2004; Geweke, 1982). Therefore the estimated causal modulations can be decomposed into different frequency ranges. When applied to fMRI, the sensitivity and specificity of such spectral Granger analysis is limited by the signal-to-noise ratio of fMRI BOLD signals at different frequencies. The spectral property of BOLD fMRI has

been studied since the early days of fMRI (Weisskoff et al., 1993). Disturbances due to cardiac/respiratory fluctuations at characteristic frequencies (Beckmann et al., 2005; Birn et al., 2006) and low frequency drift (0–0.015 Hz) (Smith et al., 1999) have been reported. Interestingly, there is also empirical evidence suggesting that BOLD signal between 0.03 Hz and 0.06 Hz can be closely related to electrophysiological activity (Zuo et al., 2010) and gives greater small-world topology (Achard et al., 2006).

In this study, we use magnetic resonance inverse imaging (InI), a method of fast fMRI capable of sampling the whole-brain BOLD signal at 10 Hz with approximately 5 mm spatial resolution at cortex using a 32-channel head coil array at 3 T (Lin et al., 2006, 2008), to study the Granger causality spectrally up to 5 Hz. We specifically hypothesize that, at frequencies higher than 1 Hz, BOLD signals can still be used to provide estimates of directional information faithfully. Using a visuomotor two-choice reaction-time task, we first successfully identified clear feed-forward effective connectivity from visual to sensorimotor systems in our previous studies (Lin et al., 2013, 2014). Such feed-forward connectivity remains significant at frequencies up to 3 Hz. Our results suggest that the BOLD signal at frequencies higher than 2 Hz can still carry useful physiological information to disclose causal modulation.

Methods

Subjects and the task

Twenty-three subjects were recruited to this study with written informed consents approved by the Institute Review Board of National Taiwan University Hospital. Subjects were all right-handed. Part of this data set was used in previous analyses (Lin et al., 2013, 2014).

The experiment used a two-choice reaction-time task, where left or right visual hemifield reversing (8 Hz) checkerboard stimuli were presented to the subjects in a rapid event-related fMRI design. The hemifield checkerboard subtended a 4.3° visual angle and was generated from 24 evenly distributed radial wedges and eight concentric rings of equal width. The stimuli were presented using Psychtoolbox (Brainard, 1997; Pelli, 1997). Stimulus duration was 500 ms; the onset of each presentation was randomized with a uniform distribution of inter-stimulus intervals varying from 3 to 16 s (average 10 s). The subjects were instructed to press the button upon detecting a visual stimulus, presented randomly at the left or right side of the screen, with the hand ipsilateral to the visual stimulus. The reaction times were recorded. Reaction times from two subjects were unavailable due to problems of the response button box.

To ensure that the estimated information flows were indeed related to the visuomotor task rather than due to spontaneous activity, we also measured the resting-state fMRI data from nine subjects. In this resting-state measurement, subjects were instructed to stay awake in the scanner. A visual crosshair was shown to the subject for 4 min.

MRI acquisition and reconstruction; region-of-interest identification and time series preparation

We used inverse imaging method to acquire BOLD-contrast fMRI with 10 Hz sampling rate. Specifically, a reference scan of InI (TR = 100 ms, TE = 30 ms, flip angle = 30°, bandwidth = 2604 Hz, FOV 256 mm × 256 mm × 256 mm; 64 × 64 × 64 image matrix) was acquired before four runs of the accelerated scan, which used the same imaging parameters of a reference except that all partition encoding steps along the left-right direction were discarded. Structural images for each subject were acquired using a 3D T_1-weighted pulse sequence (MP-RAGE: TR/TE/TI = 2,530/3.49/1100 ms, flip angle = 7°, partition thickness = 1.33 mm, image matrix = 256 × 256, 128 partitions, field-of-view = 21 cm × 21 cm). The location of the gray–white matter boundary for each participant was estimated with an automatic

segmentation algorithm to yield a triangulated mesh model with approximately 340,000 vertices (Dale et al., 1999; Fischl et al., 1999b, 2001). This cortical model was then used to facilitate mapping of the structural image from native anatomical space to a standard cortical surface space (Dale et al., 1999; Fischl et al., 1999b). Between-subject averaging was done by morphing individual data through a spherical coordinate system (Fischl et al., 1999a) implemented in FreeSurfer (https://surfer.nmr.mgh.harvard.edu).

The reconstruction of InI data was done by the minimum-norm estimate (Lin et al., 2006, 2008), which generated 2400 volumes of brain images for each 4-minute run. We used General Linear Model with finite impulse response bases function to estimate the hemodynamic responses elicited by the visuomotor task. Five regions-of-interest (ROIs) were identified from the spatial distribution of the temporally average (4 s and 7 s after visual stimulus onset) t statistics greater than 4.0 (Bonferroni corrected p-value < 0.05): visual cortex, posterior parietal cortex, pre-motor cortex, somatosensory cortex, and motor cortex. The spatial distribution of these ROIs and the associated hemodynamic responses from each ROI were reported previously (Lin et al., 2014). We extracted the raw time series (2400 samples per run) from these 5 ROIs for the subsequent causality analysis. To suppress physiological noise including cardiac and respiratory cycles, we used a Bayesian estimation tool (Sarkka et al., 2012) to automatically trace and remove these two oscillatory signals from the time series. Furthermore, we used a polynomial up to the 2nd order and sinusoidal functions (sines and cosines) with 1, 2, and 3 half-cycles to remove potential signal drifts not related to brain activity. After these pre-processing, all time series in an ROI were averaged as a single time series for each subject.

Granger causality analysis in the frequency domain

The time series from p regions can be represented as a $\mathbf{x}(t) = [x_1(t), x_2(t), ..., x_p(t)]^T$, where the superscript T denotes the transpose of a matrix/vector. Using a multi-variate auto-regressive (MVAR) model of order m to describe $\mathbf{x}(t)$, we have

$$\sum_{k=0}^{m} \boldsymbol{A}_k \boldsymbol{x}(\boldsymbol{t} - \boldsymbol{k}) = \epsilon(\boldsymbol{t}) \tag{1}$$

where $\boldsymbol{\varepsilon}(t)$ is the noise process with a covariance matrix Σ and $\mathbf{A}_k$ are $p \times p$ coefficient matrices. In practice, we used the ARFIT algorithm (Neumaier and Schneider, 2001; Schneider and Neumaier, 2001) to estimate coefficient matrices $\mathbf{A}_k$, noise covariance matrix Σ, and the optimal model order, which was jointly determined by model fitting (i.e., favoring the model with smaller power of the residual time series after fitting) and model parsimoniousness (i.e., favoring a lower order model).

The spectral matrix at frequency f can be then defined as

$$S(f) = \langle x(f) x^*(f) \rangle = H(f) \Sigma H^*(f) \tag{2}$$

where the asterisk denotes matrix transpose and taking the complex conjugate. $\mathbf{H}(f)$ is the transfer function.

$$H(f) = (\Lambda(f))^{-1} = \left(\sum_{k=0}^{m} A_k e^{-2\pi j k f} \right)^{-1} \tag{3}$$

The spectral domain formulation of the Granger causality at frequency f from region 2 to region 1 can be calculated as (Geweke, 1982):

$$I_{2 \to 1}(f) = -\ln \left(1 - \frac{\left(\Sigma_{22} - \Sigma_{12}^2 / \Sigma_{11} \right)}{S_{11}(f)} |H_{12}(f)| \right). \tag{4}$$

The formulation above did not control the information flow through indirect connections. To circumvent this problem, we chose "isolated effective coherence" (iCoh) (Pascual-Marqui et al., 2014) to describe the

direct causal modulation between two regions. Using the same MVAR model, such causal modulation at frequency f from region 2 to region 1 can be calculated as (Pascual-Marqui et al., 2014):

$$iCoh_{2\to1}(f) = \frac{\Sigma_{11}^{-1}|\Lambda_{12}(f)|^2}{\Sigma_{11}^{-1}|\Lambda_{12}(f)|^2 + \Sigma_{22}^{-1}|\Lambda_{22}(f)|^2}. \qquad (5)$$

Similar to previous Granger causality studies using fMRI data, we calculated the difference between a pair of the causality estimates between two regions in order to infer the dominant direction of the information flow:

$$dI_{2\to1}(f) = I_{2\to1}(f) - I_{1\to2}(f), \qquad (6a)$$

$$diCoh_{2\to1}(f) = iCoh_{2\to1}(f) - iCoh_{1\to2}(f). \qquad (6b)$$

The statistical inference of the dominant direction of the information flow ($dI_{2\to1}(f)$ and $diCoh_{2\to1}(f)$) was estimated by a non-parametric approach because the null distributions of both $dI_{2\to1}(f)$ and $diCoh_{2\to1}(f)$ have no analytic form. Specifically, surrogate time series were generated by the Adjusted Amplitude Fourier Transform (AAFT) algorithm, which ensures that the surrogate time series preserves the linear correlation structure of the original time series and the marginal distribution (Theiler et al., 1992). We created 100 surrogate time series and calculated $dI_{2\to1}(f)$ and $diCoh_{2\to1}(f)$. Under the null hypotheses that $dI_{2\to1}(f) = 0$ and $diCoh_{2\to1}(f) = 0$ with associated alternative hypotheses $dI_{2\to1}(f) > 0$ and $diCoh_{2\to1}(f) > 0$, we defined the p-value as the number of occurrences of $dI_{2\to1}(f)$ and $diCoh_{2\to1}(f)$ estimated from surrogate time series exceeding $dI_{2\to1}(f)$ and $diCoh_{2\to1}(f)$ estimated from the original time series, respectively. All Granger and isolated effective coherence measures were first calculated for each run and each subject and then averaged across subjects and runs of measurements. In other words, we used fixed-effect analysis to derive statistical inferences for the group-level results. We used Family-wise Discovery Rate (FDR) to control the expected proportion of false positives (Nichols and Hayasaka, 2003) when we presented results of multiple dominant directions of information flow.

The spectral analysis of the Granger causality and isolated effective coherence revealed the relative contributions of frequency components in the effectiveness of reducing prediction errors of the time series at the target region using the time series at the source region. We hypothesized that high- and low-frequency components of the time series may be best represented by different time series models. To test this hypothesis, we high-pass and low-pass filtered the time series using finite-impulse response filters and then calculated the time-domain Granger causality. Specifically, the cut-off frequency $f_{cut-off}$ was set to 0.1 Hz for the low-pass filter, and set to 0.5 Hz, 1.5 Hz, and 3.5 Hz for three different high-pass filters. In these analyses, the orders of AR were the same as those in analyzing the unfiltered time series in order to avoid potential bias because of AR model order selection.

Lastly, we also estimated the power spectral density using a multi-taper method (Dhamala et al., 2008). Specifically, the time-bandwidth product for the discrete prolate spheroidal sequences used as the data window was set to 3.5. All calculations were done using Matlab (Mathworks, Natick, MA, USA).

Results

The orders of AR model for all time series were listed in Table 1. On average, the time series were modeled with a 10- to 15-order AR model. Note that from the formulation (Eq. (3)), only one specific AR model was used for one set of the time series. In other words, the AR model order did not change across frequencies.

Fig. 1 shows the significant ($p < 0.05$) dominant directions of information flow estimated by Granger causality and isolated effective coherence at 0.1 Hz, 2.5 Hz, and 5.0 Hz. For comparison, the time

Table 1
The median of the optimal AR model order for the time series at visual cortex (V), posterior parietal cortex (PPC), premotor cortex (Premotor), somatosensory cortex (S), and motor cortex (M) across subjects.

	ROI	Median
Left hemisphere	V	14
	PPC	15
	Premotor	15
	S	13
	M	13
Right hemisphere	V	15
	PPC	10
	Premotor	12
	S	10
	M	11

domain analysis of Granger causality (Lin et al., 2014) was also shown. Note that at 0.1 Hz there was no significant causal modulation at both hemispheres. At 2.5 Hz, very similar feed-forward connections to time domain analysis were identified by both Granger causality and iCoh, particularly the dominant direction of information flow from the visual cortex to all the other four ROIs. Most of these connections at the left hemisphere remained significant up to 5.0 Hz, regardless of Granger causality or iCoh estimates. At right hemisphere, the visual → motor cortices modulation was insignificant, but visual → premotor cortices modulation was significant in Granger causality analysis. Isolated effective coherence analysis found significant PPC → premotor and somatosensory → motor cortices modulations at 5.0 Hz.

Fig. 2 shows the $dI_{2\to1}(f)$ (Fig. 2A) and $diCoh_{2\to1}(f)$ (Fig. 2B) at frequencies between 0.1 Hz and 5.0 Hz. Strong causality modulations were estimated at about 1 Hz and 2.5 Hz. Fig. 3 shows statistical significance of the dominant direction of information flow for all 10 pairs of ROIs at frequencies between 0.1 Hz and 5.0 Hz estimated by the Granger causality (Fig. 3A) and by iCoh (Fig. 3B). At the lowest frequency of 0.1 Hz, there was only one significant dominant direction of information flow from the visual to somatosensory cortex in the left hemisphere. The right hemisphere started to show significant feed-forward connection at 1.0 Hz. Between 1.0 Hz and 3.0 Hz, there were 4–7 pairs of ROIs out of total 10 pairs showing significant feed-forward connectivity at the left hemisphere. Significant information flows from the right visual cortex to other ROIs were found between 1.0 Hz and 3.0 Hz. While the number of significant feed-forward connectivity at the right hemisphere is smaller than that in the left hemisphere at frequency higher than 3.0 Hz, the dominant information flow from PPC to pre-motor cortex was still significant.

Isolated effective coherence at the left and right hemisphere showed similar results to Granger causality: there was no significant dominant direction of information at 0.1 Hz. At the left hemisphere, most significant modulations from the visual cortex to other areas in Granger causality analysis between 1 Hz and 3 Hz were also significant in iCoh analysis. At the right hemisphere, significant feed-forward connectivity identified by Granger causality were found mostly significant in iCoh analysis between 1 Hz and 3 Hz. Six out of ten possible feed-forward connectivity were significant at right hemisphere at 2.5 Hz. We also observed that significant causal modulation estimated by Granger causality at frequency higher than 3 Hz remained significant in iCoh estimates. At 5.0 Hz, iCoh indicated that there were still four and two significant feed-forward connectivity out of 10 possible pairs at the left and right hemisphere respectively.

Fig. 4 shows statistical significance of the information flow from visual to motor cortices at left and right hemispheres as a function of frequency between 0.1 Hz and 5 Hz using Granger causality (Fig. 4A) and iCoh (Fig. 4B) using measurements during the visuomotor task and resting state. These curves delineated significant visual → motor cortex modulation at different frequencies: Granger causality suggested that such modulation became significant at 0.7 Hz. This connection remained significant up to 5 Hz, the highest frequency limited by our
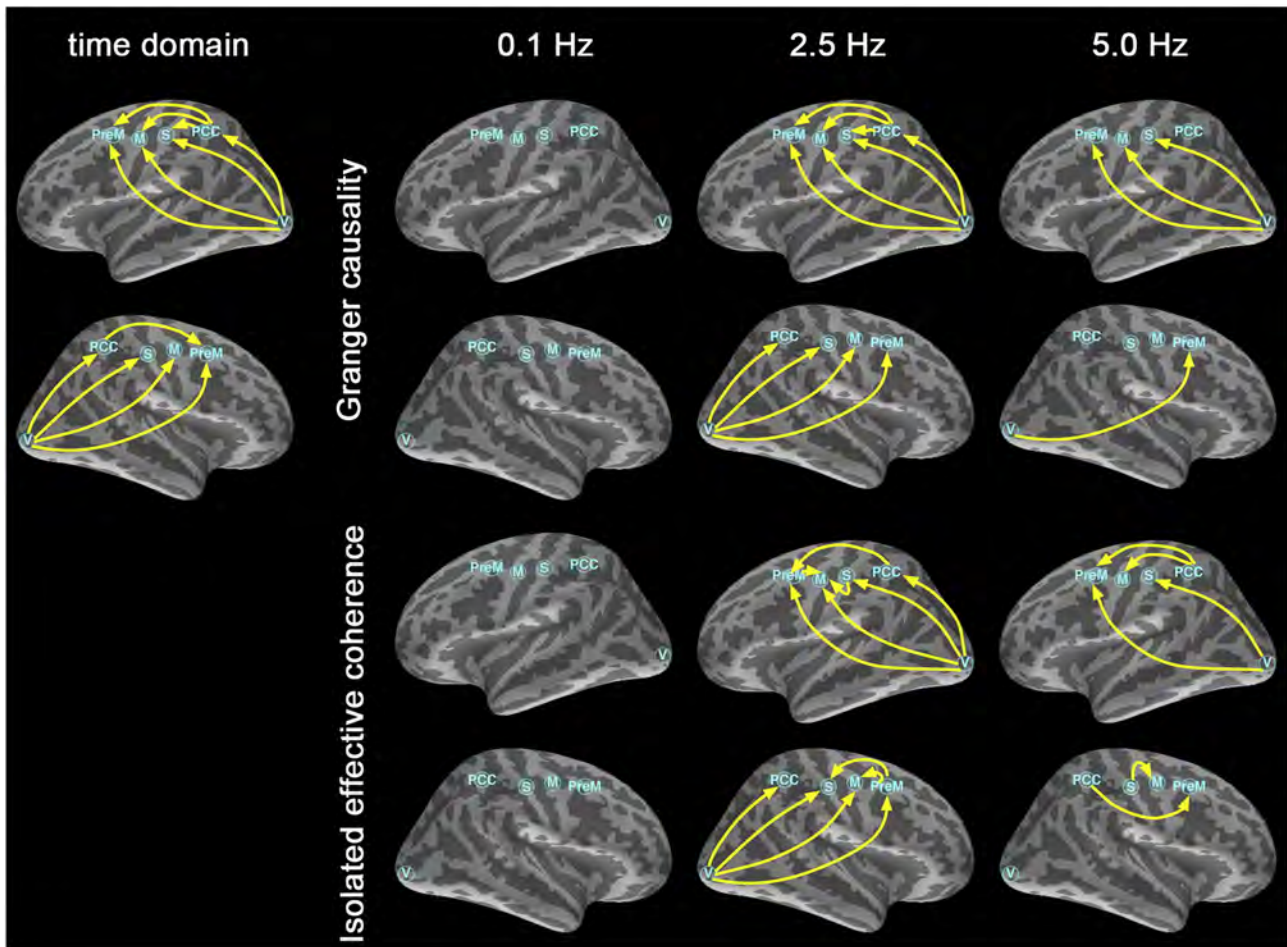
Fig. 1. Significant (corrected *p* < 0.05) dominant directions of information flow estimated by Granger causality and isolated effective coherence (iCoh) at 0. 1 Hz, 2.5 Hz, and 5.0 Hz. For comparison, the time domain analysis of Granger causality was also shown here.

inverse imaging sampling rate (10 Hz) at the left hemisphere. At the right hemisphere, this feed-forward connectivity became insignificant between 1.6 Hz and 2.0 Hz and no longer significant at frequencies higher than 3.0 Hz. Note that the spectral analysis of the resting state data did not show significant visual → motor cortex modulation in most frequencies and in both experimental conditions, except between 1.9 Hz and 2.1 Hz at the left hemisphere. Our findings suggest that this feed-forward connectivity is specific to the visuomotor task, rather than because of spontaneous fluctuations in the BOLD signal.

The significance of the visual → motor cortex modulation estimated by iCoh was found very similar to the Granger causality analysis. While there were some differences, both methods showed that only at frequency higher than 0.7 Hz, the feed-forward connection became significant. Such a dominant direction of information flow remained significant up to 5 Hz between visual and motor cortices in the left hemisphere. Calculation at the right hemisphere showed that this connectivity was not significant between 1.7 Hz and 1.9 Hz and no longer significant at frequencies higher than 3.2 Hz.

Fig. 5 shows the statistical significance of dominant directions of information flow for all 10 pairs of ROIs at frequencies between 0.1 Hz and 5.0 Hz estimated by the Granger causality after the time series were low-pass filtered (Fig. 5A) and high-pass filtered (Fig. 5B). Note that these are time domain Granger analyses. Granger causality analysis using low-pass filtered time series (cut-off frequency $f_{\text{cut-off}}$ of 0.1 Hz) showed significant visual → motor cortex connectivity. Additionally, Granger causality analyses using different high-pass filtered time series (cut-off frequencies of 0.5 Hz, and 1.5 Hz) also showed significant visual → motor cortex connectivity. However, high-pass filtered time

series with $f_{\text{cut-off}} = 3.5$ Hz only estimated significant visual → motor cortex connectivity in the left hemisphere, consistent with our spectral analysis results (Figs. 2, 3 and 4).

We performed the split-half analysis to estimate the stability of spectral analysis results. Fig. 6 shows the significant visual → motor cortex connectivity estimated by Granger causality from two random subgroups of the subjects. Right-hemisphere visual → motor cortex connectivity was singificant at about 1 Hz and 2.5 Hz. Left-hemisphere visual → motor cortex connectivity was mostly singificant above 0.8 Hz, except at two discrete ranges around 2 Hz and between 3 Hz and 4 Hz in one of the subgroups, which had a lower signal-to-noise ratio than data from all subjects. In short, the spectral signatures of the visual → motor cortex connectivity were found consistent between the split-half analysis and the analysis using all subjects (Fig. 4). The quantized *p* values in Fig. 6 were due to the numerical estimation using bootstrapping: in cases where the estimated *p*-value = 0, because there was no sample in the null distribution approximated by bootstrap samples giving a statistic higher than that from the empirical data samples, we arbitrarily assigned their *p* values equal to the least non-zero *p* value.

Figs. 7A and B show the visual → motor cortex Granger causality estimates across frequencies from all subjects in the left and right hemispheres, respectively. These causality estimates were correlated with reaction times to probe if there is any relationship. Fig. 7C shows *p*-values of these correlation analyses across frequencies. However, no significant correlation was found. The reaction times from individual subjects were shown in Fig. 8A. Specifically, the average and standard deviation of the reaction time for left- and right-hemifield visual
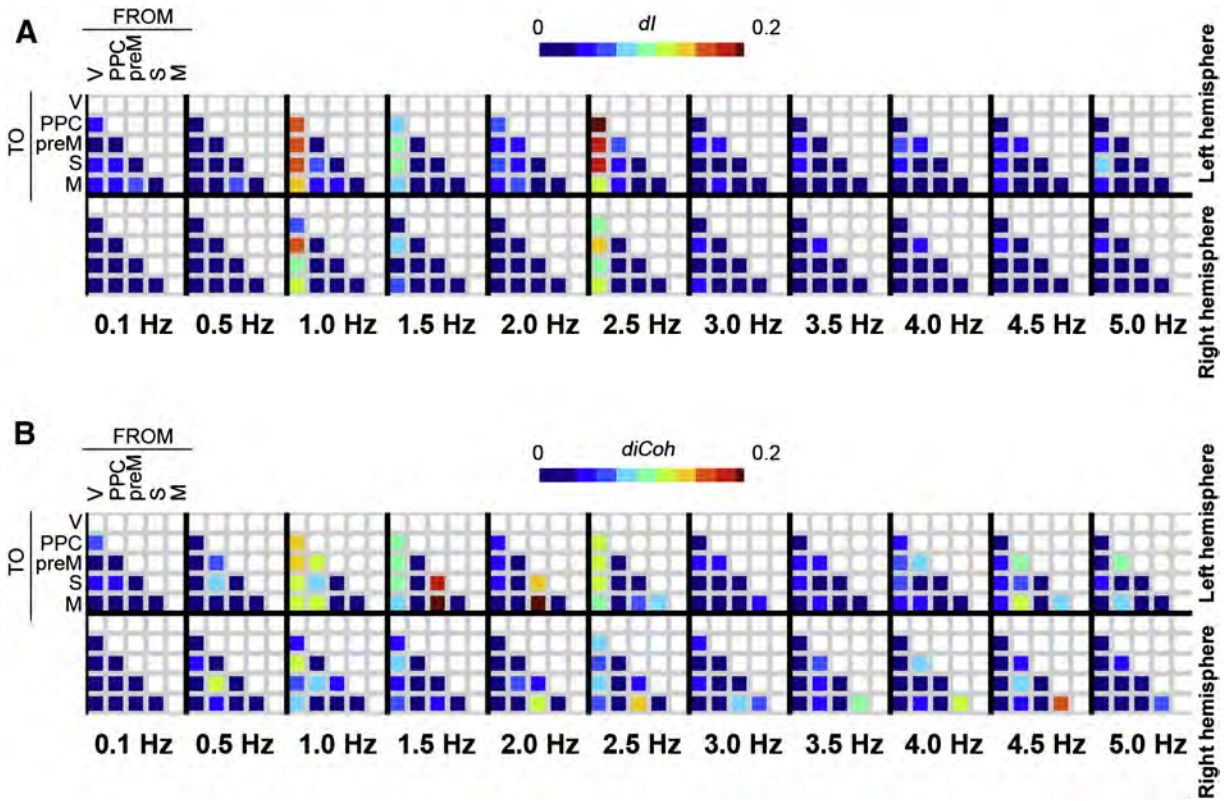
Fig. 2. The dominant directions of information flow for all 10 pairs of ROIs at frequencies between 0.1 Hz and 5.0 Hz estimated by the Granger causality (A) and iCoh (B). Causality measures were coded by color.
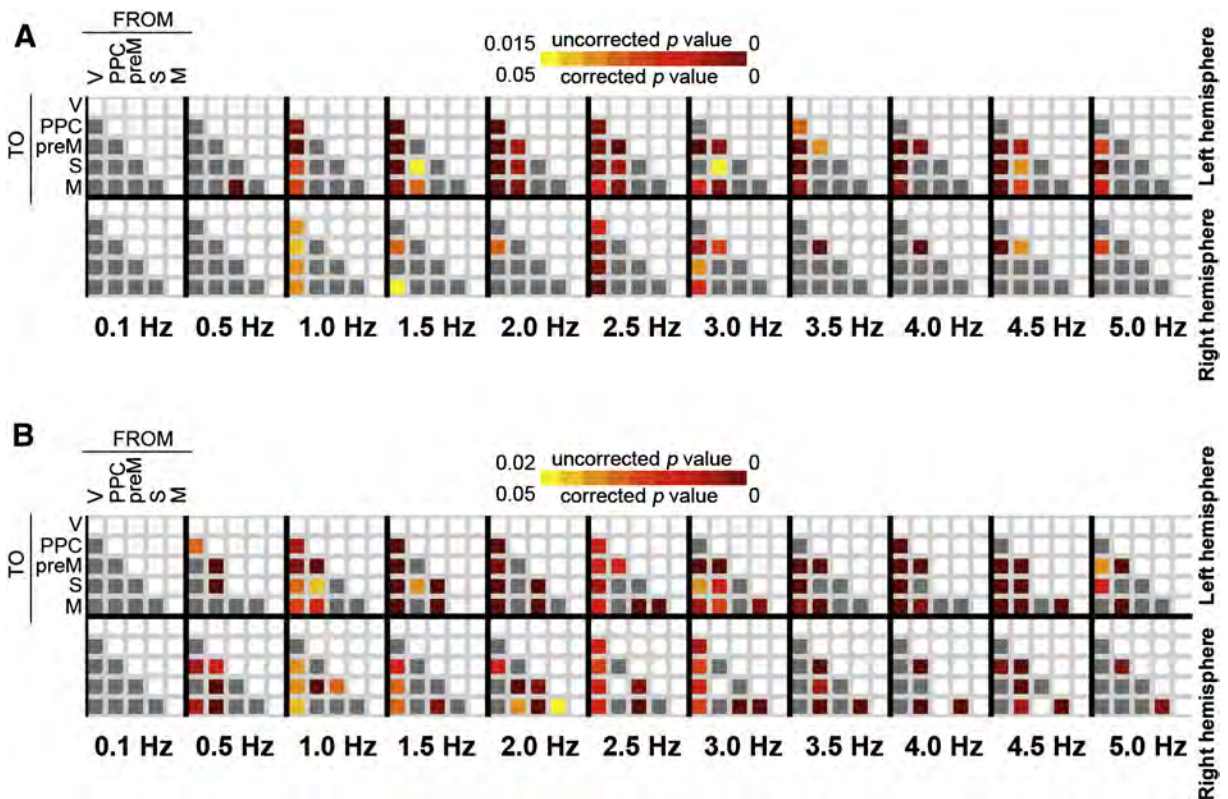

Fig. 3. Statistical significance of the dominant directions of information flow for all 10 pairs of ROIs at frequencies between 0.1 Hz and 5.0 Hz estimated by the Granger causality (A) and iCoh (B). *P*-values were coded by color. Gray color represents that the corrected *p*-values were higher than 0.05.
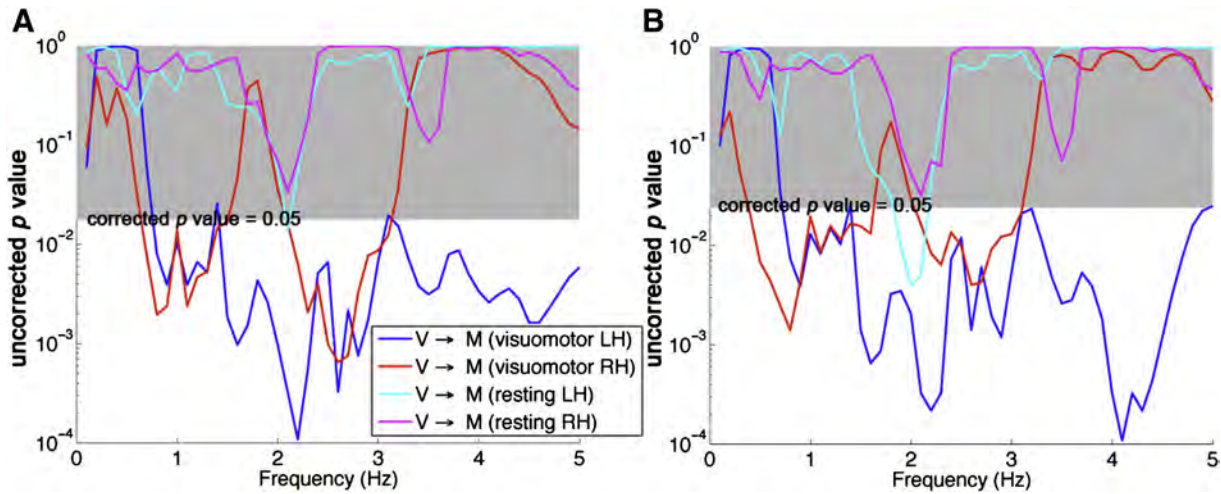
Fig. 4. Statistical significance of information flow from visual to motor cortices at left and right hemispheres as a function of frequency between 0.1 Hz and 5 Hz using Granger causality (A) and iCoh (B) during the visuomotor task and the resting state. *P*-values in the grey areas were considered insignificant.

stimulation were 350 ms $+/-$ 49 ms and 356 $+/-$ 45 ms, respectively. The difference between RTs in these two experimental conditions was insignificant (*t*-test: T = 0.452, D.O.F. = 40, *p* = 0.65). Fig. 8B shows the estimated power spectral density at ROIs. Overall, the PSD declined at higher frequencies. Peaks at about 0.2 Hz may be due to respiration. Peaks at about 1 Hz, potentially related to cardiac cycles, were found widely spread over frequencies. Visual cortex also showed strong power at 2.5 Hz. These peaks may be related to our causality findings.

Discussion

This study is the first systematic study in revealing hemodynamic causal modulations among brain areas in a task-related network at frequencies up to 5 Hz. Importantly, taking the time domain analysis results as the reference, many feed-forward connections remained significant in the same direction between 1 Hz and 3 Hz. To minimize confounds of the physiological noise from cardiac and respiratory cycles, we used a Bayesian estimation approach (Sarkka et al., 2012) to track and suppress associated spectral components. Causal modulations were found in the visuomotor functional areas in both the left and right hemispheres, contralateral to the visual stimuli and the responding hands. Additionally, these causal modulations were consistent between estimates derived from Granger causality (Geweke, 1982) and isolated effective coherence (Pascual-Marqui et al., 2014). Note that the feed-

forward connections reported here were consistent with our previous study showing correlations between the hemodynamic responses and the neuronal timing measured by magnetoencephalography (MEG) (Lin et al., 2013) as well as the time domain Granger causality calculations (Lin et al., 2014). The specificity of the estimated feed-forward connectivity to tasks was supported by the insignificant visual → motor cortex modulation during the resting-state (Fig. 4). These spectral properties were also found stable in the split-half analysis (Fig. 6). Taken together, our results suggest that hemodynamic responses carry physiological information related to inter-regional modulation at frequencies higher than what has been commonly considered. The high-frequency Granger causality shown in our study may be due to the drop of both signal and noise strength such that the signal-to-noise ratio remained comparable to that in the low frequencies. This feature was also recently reported in a resting-state fMRI study (Chen and Glover, 2015).

We need to clarify that the spectral analysis of the Granger causality and isolated effective coherence reveal the relative contributions of frequency components in reducing prediction error of the time series at the target region using the time series at the source region. The insignificant contribution of the low-frequency (≤0.1 Hz) components shown in our results (Figs. 1, 3, and 4) is indeed intriguing. One possible explanation is that high- and low-frequency components of the time series may be best represented by different models, and Granger
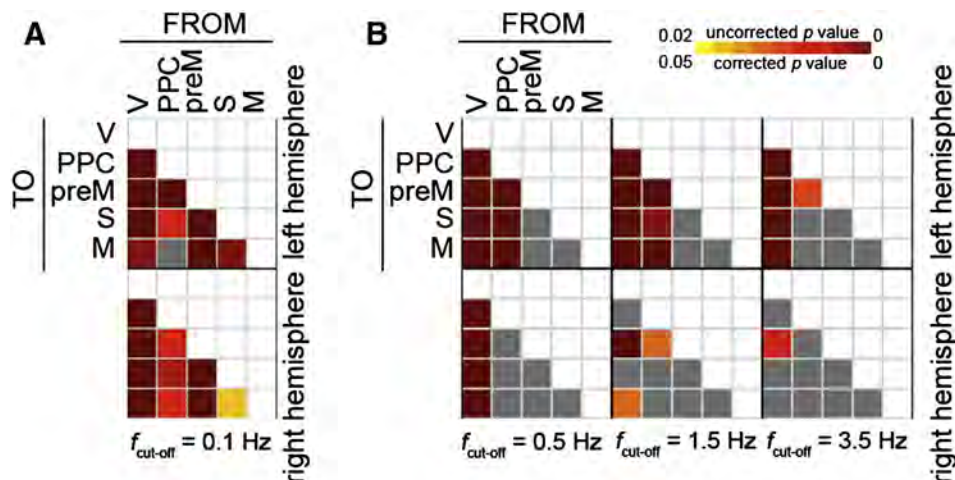

Fig. 5. The statistical significance of the dominant direction of the information flow for all 10 pairs of ROIs at frequencies between 0.1 Hz and 5.0 Hz estimated by the Granger causality after low-pass filtering (A) and high-pass filtering (B) the time series.
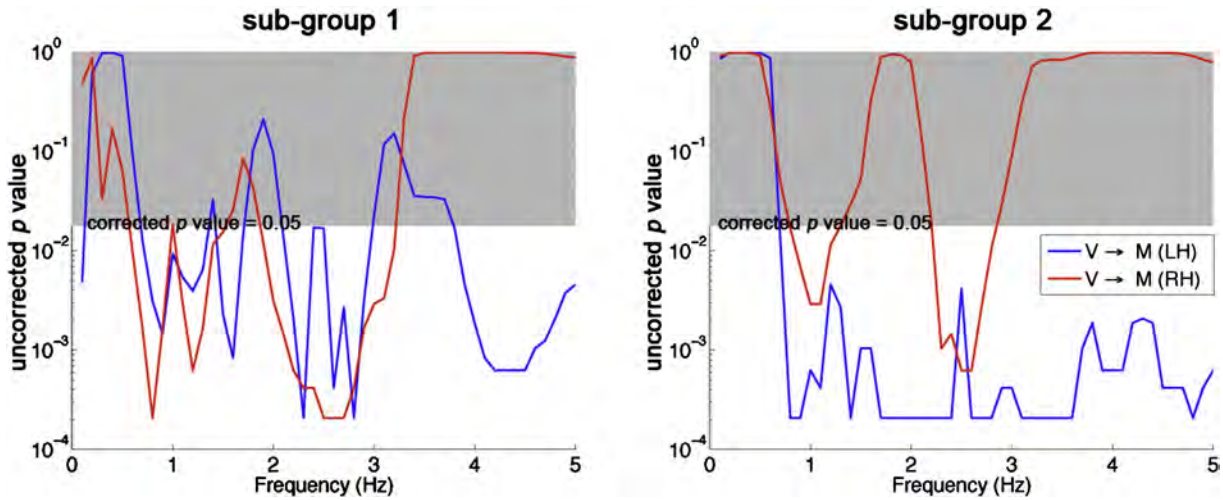
Fig. 6. The significance of visual → motor cortex connectivity estimated by Granger causality from two random sub-groups of the subjects.

causality/isolated effective coherence modeling using unfiltered time series is biased toward the high frequency components. In fact, this hypothesis is supported by the time-domain Granger causality calculations using high-pass and low-pass filtered time series (Fig. 5). Specifically, these results suggest: 1) different time series models are required for different spectral components of the time series, 2) low-frequency components ≤0.1 Hz) of the time series alone suggest the expected feed-forward connectivity (Fig. 5A), and 3) higher frequency components (>1 Hz) of the BOLD signal can still faithfully represent the causal modulations estimated by the raw time series (Fig. 5B).

Fig. 4 shows that visual → motor cortex Granger causality estimates was only significant at the left hemisphere but not at the right hemisphere at around 2 Hz. We hypothesize that this result may be related to the handedness because all subjects in this study were right handed. Further studies are required to test this hypothesis.

A recent study shows that the spatial distribution of BOLD signal varies across frequencies. Specifically, low frequency (0.01 Hz– 0.05 Hz) signals are mostly clustered in the frontal, parietal, and occipital cortex, while higher frequency (0.15 Hz–0.20 Hz) components are more prominent at temporal and cingulate cortex as well as subcortical areas (Baria et al., 2011). Such frequency-specific spatial distributions were also reported in other studies (Salvador et al., 2008; Zuo et al., 2010). Baria et al. (2011) further elucidated an interesting functional-anatomical relationship: the proportion of high frequency BOLD oscillations increases in areas at higher processing hierarchy. The interest in the spectral properties of the BOLD signal was also extended to functional connectivity studies. Specifically, there have been reports

analyzing the spectral components of the BOLD signal in the default-mode (DMN) and other networks using typical EPI with TR = 2 s (Baria et al., 2011; Chang and Glover, 2010; Salvador et al., 2008; Zuo et al., 2010) and fast MRI method (Lee et al., 2013), which can estimate frequency components up to 0.5 Hz and 5 Hz, respectively. Frequency-dependent subcomponents were identified in the DMN network (Barbaresi et al., 1995). The high frequency components of the resting-state network nodes show clear non-stationary coupling (Barbaresi et al., 1995). More stable functional connectivity was found at the higher frequency components in the visual and somatosensory networks (Lee et al., 2013). A recent resting-state fMRI study also reported frequency-dependent default-mode network and executive control network topology (Chen and Glover, 2015). These emerging evidences suggest that BOLD signals can carry distinct neurophysiological information in different frequency bands.

Our study can be considered as a natural extension of the efforts exploring spectral properties of the BOLD signal described above. Different from investigating the causality modulation in the default-mode network using typical EPI (Di and Biswal, 2014), we used a fast fMRI method to investigate frequency components of BOLD signals up to 5 Hz and to study the causal modulations between areas subserving visuomotor task.

The significant causal modulations at specific frequencies revealed in this study belong to the "delta" band (below 4 Hz) in classical electroencephalography (EEG) studies. Previously, it was found that the BOLD signal can be modulated by intermittent rhythmic delta activity induced by hyper-ventilation (Makiranta et al., 2004). The correlation
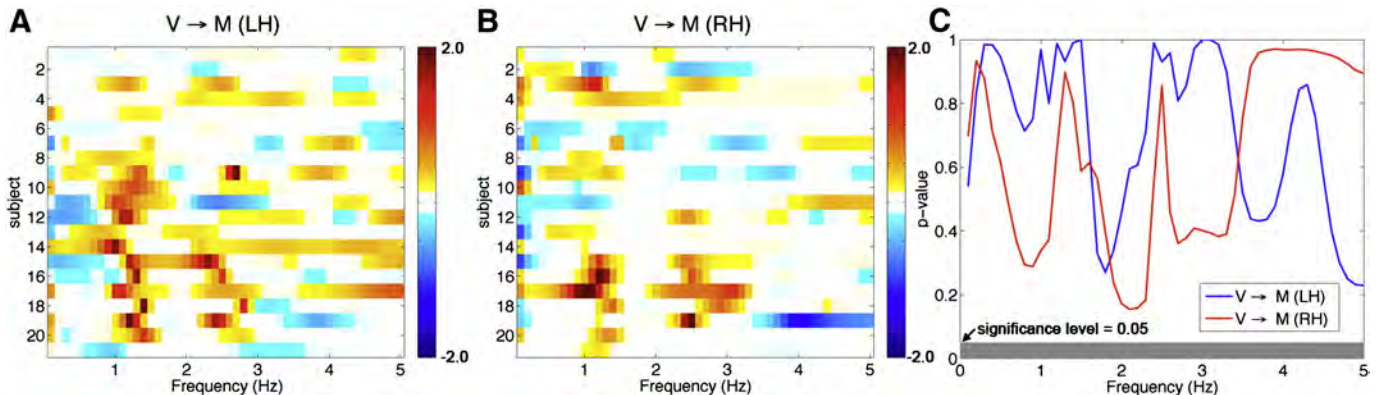

Fig. 7. The visual → motor cortex Granger causality estimates across frequencies from all subjects in the left (A) and right (B) hemispheres. (C): P-values of the correlation between the visual → motor cortex Granger causality estimate and reaction time cross frequencies.
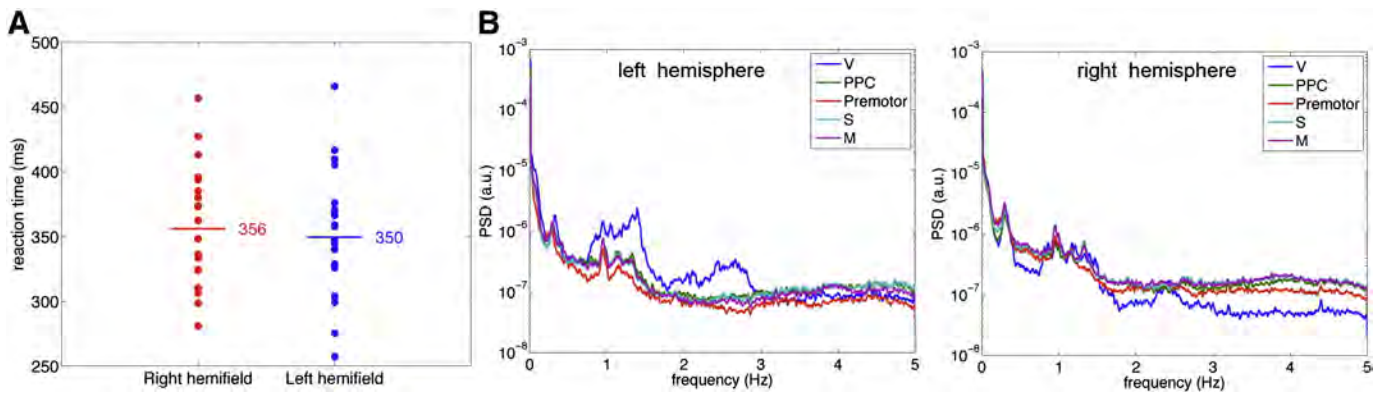
Fig. 8. (A) The reaction time of subjects in the visuomotor task using left and right hemifield visual stimulation. (B) The average power spectral density at visual cortex (V), posterior parietal cortex (PPC), premotor cortex (Premotor), somatosensory cortex (S), and motor cortex (M).

between the delta band oscillations at the anterior cingulate cortex in the DMN and the BOLD response at the parahippocampal gyrus was also reported in a simultaneous EEG-fMRI study (Neuner et al., 2014). Our finding corroborated a recent animal study showing a tight coupling between the low frequency components of the local field potential between bilateral whisker barrel cortices in rats (Lu et al., 2014). These results altogether suggest a plausible neurovascular coupling at the delta band. However, it should be kept in mind that our results should not be interpreted as the neuronal information flow, as the BOLD signal has been considered as a subsequent vascular event after neuronal activity (Logothetis et al., 2001).

Our analysis decomposed the time-domain causal modulation between ROIs into individual frequency bands. However, our decomposition ignores the potential interaction across frequencies. As it has been suggested in EEG and MEG analyses, neuronal activity can interact via complex phase-amplitude and power coupling at different frequencies (Canolty and Knight, 2010). We speculate that the BOLD signal may also demonstrate similar cross-frequency modulations at the resting state or in response to exogenous stimuli. This hypothesis can only be answered by further studies.

Our study aims at decomposing the directional information flow into different spectral components using only cortical BOLD signal time series. Thus the contributions from sub-cortical and cerebellar structures were neglected and the effective connectivity can be biased. However, our study aims at decomposing the directional information flow into different spectral components using only cortical BOLD signal time series. In particular, the finding that the high frequency component of the Granger causality revealed the same significant feed-forward connectivity estimated in the wide-band time-domain Granger causality analysis is the new information in our study.

The AR-model orders reported in our study were between 10 and 15 (Table 1). The time series measured by typical fMRI protocols with TR of 1 or 2 s can be modeled by the first order AR model (Purdon and Weisskoff, 1998). This suggested that the hemodynamic signals are temporally correlated when measurements are taken within seconds. In InI with TR = 0.1 s, this correlation is expected among consecutive measurements of about 10 to 20 samples. Our estimated AR model supported this argument.

This study used the inverse imaging method to achieve 10 Hz sampling rate with whole-brain FOV coverage and the minimal compromise of spatial resolution (Lin et al., 2008). A similar fast MRI method, MR-encephalography (MREG) (Hennig et al., 2007), was also developed independently. Both methods allow us to explore the spectral decomposition of the BOLD signal up to 5 Hz. If spatial coverage can be limited, it is also possible to use single-slice EPI to achieve the same bandwidth. Even faster sampling can be achieved by optimizing the inverse imaging protocol (Boyacioglu and Barth, 2013) or using the echo-shifting method (Chang et al., 2013) to investigate the BOLD

signal frequency up to 10 Hz (50 ms TR). However, if the frequency components up to 2–3 Hz is sufficient, simultaneous multi-slice imaging, a method of sub-second whole-brain fMRI (Feinberg et al., 2010), may be used without compromising the spatial resolution. In summary, these methods enable the exploration of the BOLD spectrum beyond 0.5 Hz as limited by a typical 2 s TR in multi-slice EPI.

Acknowledgment

References

Abler, B., Roebroeck, A., Goebel, R., Hose, A., Schonfeldt-Lecuona, C., Hole, G., Walter, H., 2006. Investigating directed influences between activated brain areas in a motor-response task using fMRI. Magn. Reson. Imaging 24, 181–185.

Achard, S., Salvador, R., Whitcher, B., Suckling, J., Bullmore, E., 2006. A resilient, low-frequency, small-world human brain functional network with highly connected association cortical hubs. J. Neurosci. 26, 63–72.

Barbaresi, P., Guandalini, P., Manzoni, T., 1995. Laminar pattern of termination of the ipsilateral cortical projection from SII to SI in cats. J. Comp. Neurol. 360, 319–330.

Baria, A.T., Baliki, M.N., Parrish, T., Apkarian, A.V., 2011. Anatomical and functional assemblies of brain BOLD oscillations. J. Neurosci. 31, 7910–7919.

Beckmann, C.F., DeLuca, M., Devlin, J.T., Smith, S.M., 2005. Investigations into resting-state connectivity using independent component analysis. Philos. Trans. R. Soc. Lond. B Biol. Sci. 360, 1001–1013.

Belliveau, J., Kennedy, D., McKinstry, R., Buchbinder, B., Weisskoff, R., Cohen, M., Vevea, J., Brady, T., Rosen, B., 1991. Functional mapping of the human visual cortex by magnetic resonance imaging. Science 254, 716–719.

Birn, R.M., Diamond, J.B., Smith, M.A., Bandettini, P.A., 2006. Separating respiratory-variation-related fluctuations from neuronal-activity-related fluctuations in fMRI. Neuroimage 31, 1536–1548.

Boyacioglu, R., Barth, M., 2013. Generalized INverse imaging (GIN): ultrafast fMRI with physiological noise correction. Magn. Reson. Med. 70, 962–971.

Brainard, D.H., 1997. The psychophysics toolbox. Spat. Vis. 10, 433–436.

Brovelli, A., Ding, M., Ledberg, A., Chen, Y., Nakamura, R., Bressler, S.L., 2004. Beta oscillations in a large-scale sensorimotor cortical network: directional influences revealed by Granger causality. Proc. Natl. Acad. Sci. U. S. A. 101, 9849–9854.

Canolty, R.T., Knight, R.T., 2010. The functional role of cross-frequency coupling. Trends Cogn. Sci. 14, 506–515.

Chang, C., Glover, G.H., 2010. Time–frequency dynamics of resting-state brain connectivity measured with fMRI. Neuroimage 50, 81–98.

Chang, W.T., Nummenmaa, A., Witzel, T., Ahveninen, J., Huang, S., Tsai, K.W., Chu, Y.H., Polimeni, J.R., Belliveau, J.W., Lin, F.H., 2013. Whole-head rapid fMRI acquisition using echo-shifted magnetic resonance inverse imaging. Neuroimage 78, 325–338.

Chen, J.E., Glover, G.H., 2015. BOLD fractional contribution to resting-state functional connectivity above 0.1 Hz. Neuroimage 107, 207–218.

Dale, A.M., Fischl, B., Sereno, M.I., 1999. Cortical surface-based analysis. I. Segmentation and surface reconstruction. Neuroimage 9, 179–194.

David, O., Guillemain, I., Saillet, S., Reyt, S., Deransart, C., Segebarth, C., Depaulis, A., 2008. Identifying neural drivers with functional MRI: an electrophysiological validation. PLoS Biol. 6, 2683–2697.

Deshpande, G., Sathian, K., Hu, X., 2009. Effect of hemodynamic variability on Granger causality analysis of fMRI. Neuroimage 52, 884–896.

Dhamala, M., Rangarajan, G., Ding, M., 2008. Analyzing information flow in brain networks with nonparametric Granger causality. Neuroimage 41, 354–362.

Di, X., Biswal, B.B., 2014. Identifying the default mode network structure using dynamic causal modeling on resting-state functional magnetic resonance imaging. Neuroimage 86, 53–59.

Eichler, M., 2005. A graphical approach for evaluating effective connectivity in neural systems. Philos. Trans. R. Soc. Lond. B Biol. Sci. 360, 953–967.

Feinberg, D.A., Moeller, S., Smith, S.M., Auerbach, E., Ramanna, S., Gunther, M., Glasser, M.F., Miller, K.L., Ugurbil, K., Yacoub, E., 2010. Multiplexed echo planar imaging for sub-second whole brain FMRI and fast diffusion imaging. PLoS One 5, e15710.

Fischl, B., Sereno, M., Tootell, R., Dale, A., 1999a. High-resolution inter-subject averaging and a coordinate system for the cortical surface. Hum. Brain Mapp. 8, 272–284.

Fischl, B., Sereno, M.I., Dale, A.M., 1999b. Cortical surface-based analysis. II: inflation, flattening, and a surface-based coordinate system. Neuroimage 9, 195–207.

Fischl, B., Liu, A., Dale, A.M., 2001. Automated manifold surgery: constructing geometrically accurate and topologically correct models of the human cerebral cortex. IEEE Trans. Med. Imaging 20, 70–80.

Friston, K., 2011a. Dynamic causal modeling and Granger causality Comments on: The identification of interacting networks in the brain using fMRI: model selection, causality and deconvolution. Neuroimage 58, 303–305.

Friston, K.J., 2011b. Functional and effective connectivity: a review. Brain Connect. 1, 13–36.

Friston, K.J., Harrison, L., Penny, W., 2003. Dynamic causal modelling. Neuroimage 19, 1273–1302.

Geweke, J., 1982. Measurement of linear dependence and feedback between multiple time series. J. Am. Stat. Assoc. 77, 304–313.

Goebel, R., Roebroeck, A., Kim, D.S., Formisano, E., 2003. Investigating directed cortical interactions in time-resolved fMRI data using vector autoregressive modeling and Granger causality mapping. Magn. Reson. Imaging 21, 1251–1261.

Granger, C.W.J., 1969. Investigating causal relations by econometric models and cross-spectral methods. Econometrica 37, 424–438.

Hennig, J., Zhong, K., Speck, O., 2007. MR-encephalography: fast multi-channel monitoring of brain physiology with magnetic resonance. Neuroimage 34, 212–219.

Kayser, A.S., Sun, F.T., D'Esposito, M., 2009. A comparison of Granger causality and coherency in fMRI-based analysis of the motor system. Hum. Brain Mapp. 30, 3475–3494.

Kwong, K., Belliveau, J., Chesler, D., Goldberg, I., Weisskoff, R., Poncelet, B., Kennedy, D., Hoppel, B., Cohen, M., Turner, R., Cheng, H., Brady, T., Rosen, B., 1992. Dynamic magnetic resonance imaging of human brain activity during primary sensory stimulation. Proc. Natl. Acad. Sci. U. S. A. 89, 5675–5679.

Lee, A.T., Glover, G.H., Meyer, C.H., 1995. Discrimination of large venous vessels in time-course spiral blood-oxygen-level-dependent magnetic-resonance functional neuroimaging. Magn. Reson. Med. 33, 745–754.

Lee, H.L., Zahneisen, B., Hugger, T., LeVan, P., Hennig, J., 2013. Tracking dynamic resting-state networks at higher frequencies using MR-encephalography. Neuroimage 65, 216–222.

Lin, F.H., Wald, L.L., Ahlfors, S.P., Hamalainen, M.S., Kwong, K.K., Belliveau, J.W., 2006. Dynamic magnetic resonance inverse imaging of human brain function. Magn. Reson. Med. 56, 787–802.

Lin, F.H., Witzel, T., Mandeville, J.B., Polimeni, J.R., Zeffiro, T.A., Greve, D.N., Wiggins, G., Wald, L.L., Belliveau, J.W., 2008. Event-related single-shot volumetric functional magnetic resonance inverse imaging of visual processing. Neuroimage 42, 230–247.

Lin, F.H., Witzel, T., Raij, T., Ahveninen, J., Tsai, K.W., Chu, Y.H., Chang, W.T., Nummenmaa, A., Polimeni, J.R., Kuo, W.J., Hsieh, J.C., Rosen, B.R., Belliveau, J.W., 2013. fMRI hemodynamics accurately reflects neuronal timing in the human brain measured by MEG. Neuroimage 78, 372–384.

Lin, F.H., Ahveninen, J., Raij, T., Witzel, T., Chu, Y.H., Jaaskelainen, I.P., Tsai, K.W., Kuo, W.J., Belliveau, J.W., 2014. Increasing fMRI sampling rate improves Granger causality estimates. PLoS One 9, e100319.

Logothetis, N., Pauls, J., Augath, M., Trinath, T., Oeltermann, A., 2001. Neurophysiological investigation of the basis of the fMRI signal. Nature 412, 150–157.

Londei, A., D'Ausilio, A., Basso, D., Belardinelli, M.O., 2006. A new method for detecting causality in fMRI data of cognitive processing. Cogn. Process. 7, 42–52.

Lu, H., Wang, L., Rea, W.W., Brynildsen, J.K., Jaime, S., Zuo, Y., Stein, E.A., Yang, Y., 2014. Low- but not high-frequency LFP correlates with spontaneous BOLD fluctuations in rat whisker barrel cortex. Cereb. Cortex.

Makiranta, M.J., Ruohonen, J., Suominen, K., Sonkajarvi, E., Salomaki, T., Kiviniemi, V., Seppanen, T., Alahuhta, S., Jantti, V., Tervonen, O., 2004. BOLD-contrast functional MRI signal changes related to intermittent rhythmic delta activity in EEG during voluntary hyperventilation-simultaneous EEG and fMRI study. Neuroimage 22, 222–231.

McArdle, J.J., McDonald, R.P., 1984. Some algebraic properties of the Reticular Action Model for moment structures. Br. J. Math. Stat. Psychol. 37 (Pt 2), 234–251.

Miezin, F.M., Maccotta, L., Ollinger, J.M., Petersen, S.E., Buckner, R.L., 2000. Characterizing the hemodynamic response: effects of presentation rate, sampling procedure, and the possibility of ordering brain activity based on relative timing. Neuroimage 11, 735–759.

Neumaier, A., Schneider, T., 2001. Estimation of parameters and eigenmodes of multivariate autoregressive models. ACM Trans. Math. Softw. 27, 27–57.

Neuner, I., Arrubla, J., Werner, C.J., Hitz, K., Boers, F., Kawohl, W., Shah, N.J., 2014. The default mode network and EEG regional spectral power: a simultaneous fMRI-EEG study. PLoS One 9, e88214.

Nichols, T., Hayasaka, S., 2003. Controlling the familywise error rate in functional neuroimaging: a comparative review. Stat. Methods Med. Res. 12, 419–446.

Ogawa, S., Tank, D.W., Menon, R., Ellermann, J.M., Kim, S.-G., Merkle, H., Ugurbil, K., 1992. Intrinsic signal changes accompanying sensory stimulation: functional brain mapping with magnetic resonance imaging. Proc. Natl. Acad. Sci. U. S. A. 89, 5951–5955.

Pascual-Marqui, R.D., Biscay, R.J., Bosch-Bayard, J., Lehmann, D., Kochi, K., Kinoshita, T., Yamada, N., Sadato, N., 2014. Assessing direct paths of intracortical causal information flow of oscillatory activity with the isolated effective coherence (iCoh). Front. Hum. Neurosci. 8, 448.

Pelli, D.G., 1997. The VideoToolbox software for visual psychophysics: transforming numbers into movies. Spat. Vis. 10, 437–442.

Penny, W.D., Stephan, K.E., Mechelli, A., Friston, K.J., 2004. Comparing dynamic causal models. Neuroimage 22, 1157–1172.

Purdon, P.L., Weisskoff, R.M., 1998. Effect of temporal autocorrelation due to physiological noise and stimulus paradigm on voxel-level false-positive rates in fMRI. Hum. Brain Mapp. 6, 239–249.

Roebroeck, A., Formisano, E., Goebel, R., 2005. Mapping directed influence over the brain using Granger causality and fMRI. Neuroimage 25, 230–242.

Salvador, R., Martinez, A., Pomarol-Clotet, E., Gomar, J., Vila, F., Sarro, S., Capdevila, A., Bullmore, E., 2008. A simple view of the brain through a frequency-specific functional connectivity measure. Neuroimage 39, 279–289.

Sarkka, S., Solin, A., Nummenmaa, A., Vehtari, A., Auranen, T., Vanni, S., Lin, F.H., 2012. Dynamic retrospective filtering of physiological noise in BOLD fMRI: DRIFTER. Neuroimage 60, 1517–1527.

Sato, J.R., Junior, E.A., Takahashi, D.Y., de Maria Felix, M., Brammer, M.J., Morettin, P.A., 2006. A method to produce evolving functional connectivity maps during the course of an fMRI experiment using wavelet-based time-varying Granger causality. Neuroimage 31, 187–196.

Schneider, T., Neumaier, A., 2001. Algorithm 808: ARfit—a matlab package for the estimation of parameters and eigenmodes of multivariate autoregressive models. ACM Trans. Math. Softw. 27, 58–65.

Smith, A.M., Lewis, B.K., Ruttimann, U.E., Ye, F.Q., Sinnwell, T.M., Yang, Y., Duyn, J.H., Frank, J.A., 1999. Investigation of low frequency drift in fMRI signal. Neuroimage 9, 526–533.

Smith, S.M., Bandettini, P.A., Miller, K.L., Behrens, T.E., Friston, K.J., David, O., Liu, T., Woolrich, M.W., Nichols, T.E., 2012. The danger of systematic bias in group-level FMRI-lag-based causality estimation. Neuroimage 59, 1228–1229.

Stephan, K.E., Roebroeck, A., 2012. A short history of causal modeling of fMRI data. Neuroimage 62, 856–863.

Theiler, J., Eubank, S., Longtin, A., Galdrikian, B., Farmer, J.D., 1992. Testing for nonlinearity in time-series—the method of surrogate data. Phys. D 58, 77–94.

Weisskoff, R., Baker, J., Belliveau, J.W., Davis, T., Kwong, K.K., Cohen, M., Rosen, B.R., 1993. Power Spectrum Analysis of Functionally-Weighted MR Data: What's in the Noise? Proceedings of the 12th Annual Meeting of Society of Magnetic Resonance in Medicine 7

Zuo, X.N., Di Martino, A., Kelly, C., Shehzad, Z.E., Gee, D.G., Klein, D.F., Castellanos, F.X., Biswal, B.B., Milham, M.P., 2010. The oscillating brain: complex and reliable. Neuroimage 49, 1432–1445.